

Setting the clock of photoelectron emission through molecular alignment

Andrea Trabattoni,^{1,2} Sebastian Trippel,^{1,2} Umberto De Giovannini,^{3,4} Jean François Olivieri,¹ Joss Wiese,^{1,5} Terry Mullins,¹ Jolijn Onvlee,¹ Sang-Kil Son,^{1,2} Biagio Frusteri,⁴ Angel Rubio,^{3,6,7} and Jochen Küpper^{1,2,5,7}

¹Center for Free-Electron Laser Science, Deutsches Elektronen-Synchrotron DESY, Notkestraße 85, 22607 Hamburg, Germany

²The Hamburg Center for Ultrafast Imaging, Universität Hamburg, Luruper Chaussee 149, 22761 Hamburg, Germany

³Max Planck Institute for the Structure and Dynamics of Matter and

Center for Free-Electron Laser Science, Hamburg 22761 Hamburg, Germany

⁴Dipartimento di Fisica e Chimica, Università degli Studi di Palermo, Via Archirafi 36, I-90123, Palermo, Italy

⁵Department of Chemistry, Universität Hamburg, Martin-Luther-King-Platz 6, 20146 Hamburg, Germany

⁶Center for Computational Quantum Physics (CCQ), The Flatiron Institute, 162 Fifth Avenue, New York NY 10010

⁷Department of Physics, Universität Hamburg, Luruper Chaussee 149, 22761 Hamburg, Germany

(Dated: February 20, 2018)

The interaction of strong laser fields with matter intrinsically provides powerful tools to image transient dynamics with an extremely high spatiotemporal resolution. In strong-field physics, the initial conditions of this interaction are generally considered a weak perturbation. We investigated strong-field ionisation of laser-aligned molecules and showed, for the first time, that the initial momentum acquired by the photoelectron at birth has a dramatic impact on the overall strong-field dynamics: It sets the clock for the emission of electrons with a given kinetic energy. This result represents a new benchmark for the seminal statements of strong-field physics, highlighting the crucial importance of the initial electron-emission conditions. Our findings have strong impact on the interpretation of self-diffraction experiments, where the photoelectron momentum distribution is used to retrieve molecular structures. Furthermore, the resulting encoding of the time-energy relation in molecular-frame photoelectron distributions provides a new way of probing the molecular potential with sub-femtosecond resolution and accessing a deeper understanding of electron tunnelling.

In the prototypical strong-field interaction, an intense driving field extracts a valence electron from the target through tunnel ionisation, drives the free electron in vacuum, and eventually streaks it back to the parent ion, predominantly resulting in rescattering or radiative recombination [1, 2]. The radiative recombination results in the emission of high-energy photons *via* high-harmonic generation (HHG) [1] and this is a powerful tool to investigate the molecular potential with attosecond temporal resolution [3–5]. Alternatively, the rescattered portion of this electron wave packet is exploited in laser-induced electron diffraction (LIED) [6] experiments as a coherent diffraction pattern of the molecular target, potentially providing time-dependent images of the molecule at sub-femtosecond and few-picometer resolution. Recently, corresponding experimental results for the structure or dynamics of small molecules were obtained [7–10]. At the same time, the initial conditions of the strong-field interaction have attracted much attention to capture the intrinsic nature of strong-field

physics. While pioneering attosecond experiments and molecular-frame measurements revealed non-trivial spatiotemporal features in electron tunneling [11, 12], these initial conditions are still generally considered a weak perturbation in strong-field physics. All the results obtained in LIED experiments, for example, are interpreted in the framework of the strong-field approximation, where the electron is considered to be born in the continuum with a negligible initial momentum and to propagate as a plane wave [13]. Within this approach, the diffraction pattern can be analysed utilising the angular [7, 8] or radial [14] photoelectron distribution. However, the relevance of the ionised molecular orbital in the rescattered photoelectrons is still under discussion. So far, this was included by an overall weighting factor in the rescattering probability [15, 16], or as a spatial phase or an angular feature in the rescattering electron wavepacket [12, 17]. Recently, the influence of molecular alignment on molecular structure retrieval was discussed [14, 18]. However, general predictions are still extremely challenging with more models appearing [19, 20].

Here, we experimentally and computationally studied molecular-frame photoelectron spectroscopy from strongly aligned molecules in order to investigate the relation between the molecular frame and the strong-field-induced ultrafast electron dynamics. We demonstrated that the initial momentum acquired by the electron in the molecular frame sets a precise time-energy relation for the electron dynamics.

Fig. 1 depicts the experiment. An ultracold ensemble of carbonyl sulfide (OCS) molecules [21] was adiabatically aligned in the laboratory frame, with $\langle \cos^2 \theta_{2D} \rangle = 0.9$, by using a linearly polarised, 500 ps laser pulse, centered at 800 nm [22]. The molecules were aligned in two different configurations, shown in Fig. 1, with the molecular axis along the Y and Z axes, named parallel and perpendicular alignment, respectively. A second laser pulse, centered at 1300 nm, with a duration of 65 fs, and a peak intensity of $8 \cdot 10^{13}$ W/cm², was used to singly ionise the OCS molecules. For this intensity the ponderomotive energy of the laser field is $U_p \approx 13$ eV and the ionisation occurred

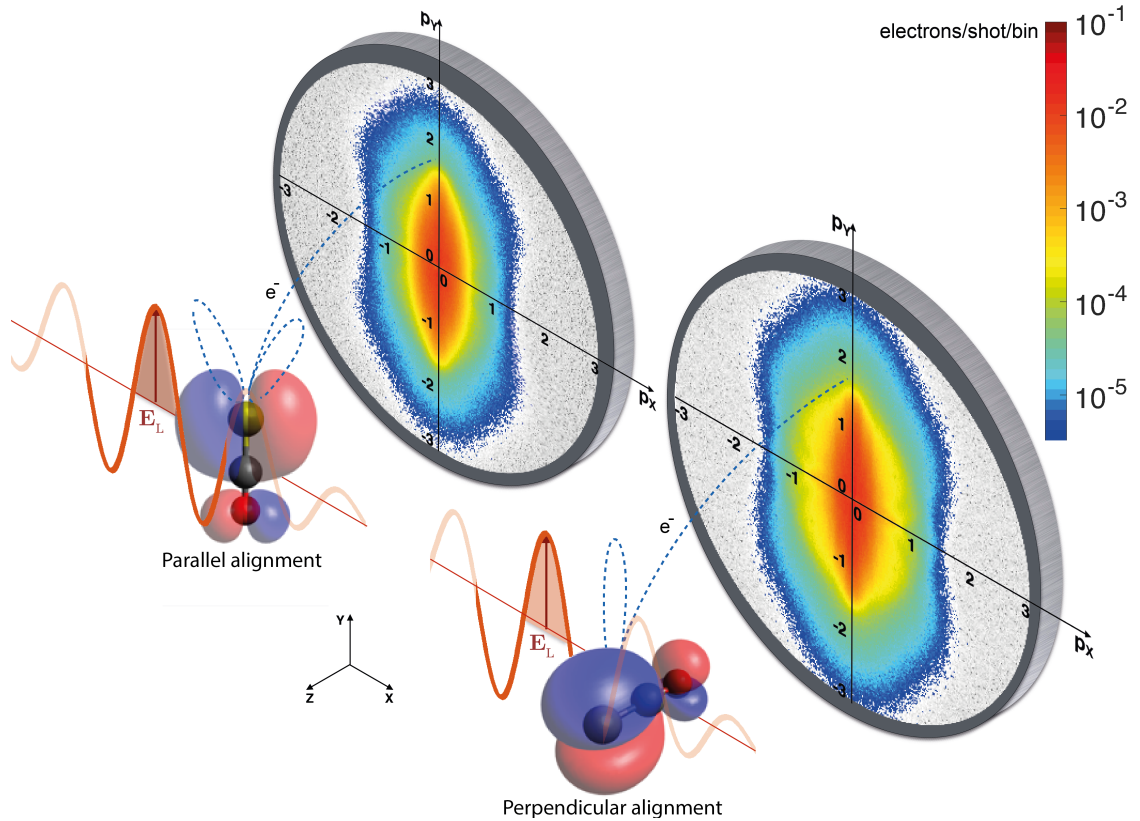


FIG. 1. Sketch of the experimental arrangement with alignment of OCS molecules in the laboratory frame, parallel and perpendicular to the Y axis. The ionising laser is linearly polarised along the Y axis and the detection is in the XY plane. The molecular-frame angle-resolved photoelectron spectra are projected onto a 2D detector in a velocity map imaging spectrometer. The spectra are displayed in units of electrons/shot/bin.

in the tunneling regime. The ionising laser pulse, \mathbf{E}_L in Fig. 1, was linearly polarised along the Y axis. The produced molecular-frame angle-resolved photoelectron spectra (MF-ARPES) were recorded in a velocity map imaging (VMI) spectrometer with its detector parallel to the XY plane. It is important to note that the de Broglie wavelength of rescattering electrons in the experiment was larger than 200 pm. In this regime no diffraction feature is expected to appear in the photoelectron distributions [14]. Fig. 1 shows the MF-ARPES for parallel (left) and perpendicular (right) alignment on a logarithmic scale, in units of electrons/shot/bin. The two distributions show several differences. The spectrum for parallel alignment has a larger width at low transverse momenta, $p_X < 0.5$ a. u. (atomic units), while the spectrum for perpendicular alignment shows a number of angular features for transverse momentum p_X between 0.5 a. u. and 1 a. u.. These angular structures, which are much weaker in the spectrum for parallel alignment, could be identified as holographic features [10, 23]. Focusing the attention on large longitudinal momenta p_Y , the counts for parallel alignment drop around 2.5 a. u. and disappear before reaching 3 a. u.. In the case of perpendicular alignment, however, the spectrum extends to higher momenta,

showing an appreciable amount of counts at $p_Y = 3$ a. u.. The drop of signal at high longitudinal momenta, namely the high energy cutoff, is expected to be dependent only on the strong-field properties [24]. Surprisingly, in the current study we found a clear dependence on the molecular frame.

To properly measure the high energy cutoff for both spectra, the two MF-ARPES were recorded for a large range of p_Y . Fig. 2 a shows a close comparison of the two experimental distributions for a range of p_Y (and p_X) between 0 and 4 a. u.. Here, the spectra were cut along the Y axis and half of each was reported in Fig. 2 a, with the spectrum from parallel alignment on the left and the one from perpendicular alignment on the right. Now, the differences at low momenta and at the cutoff are even more evident. To perform a quantitative analysis of the cutoffs, the momentum distributions along the longitudinal axis (Y) were integrated within an angle of $\pm 20^\circ$ and converted to an energy scale. In Fig. 2 b the resulting photoelectron spectra are shown for parallel (blue) and perpendicular (red) alignment, with energies in units of U_p . The perpendicular/parallel ratio of the two area-normalised spectra (green) shows a predominance of photoelectrons for perpendicular alignment in

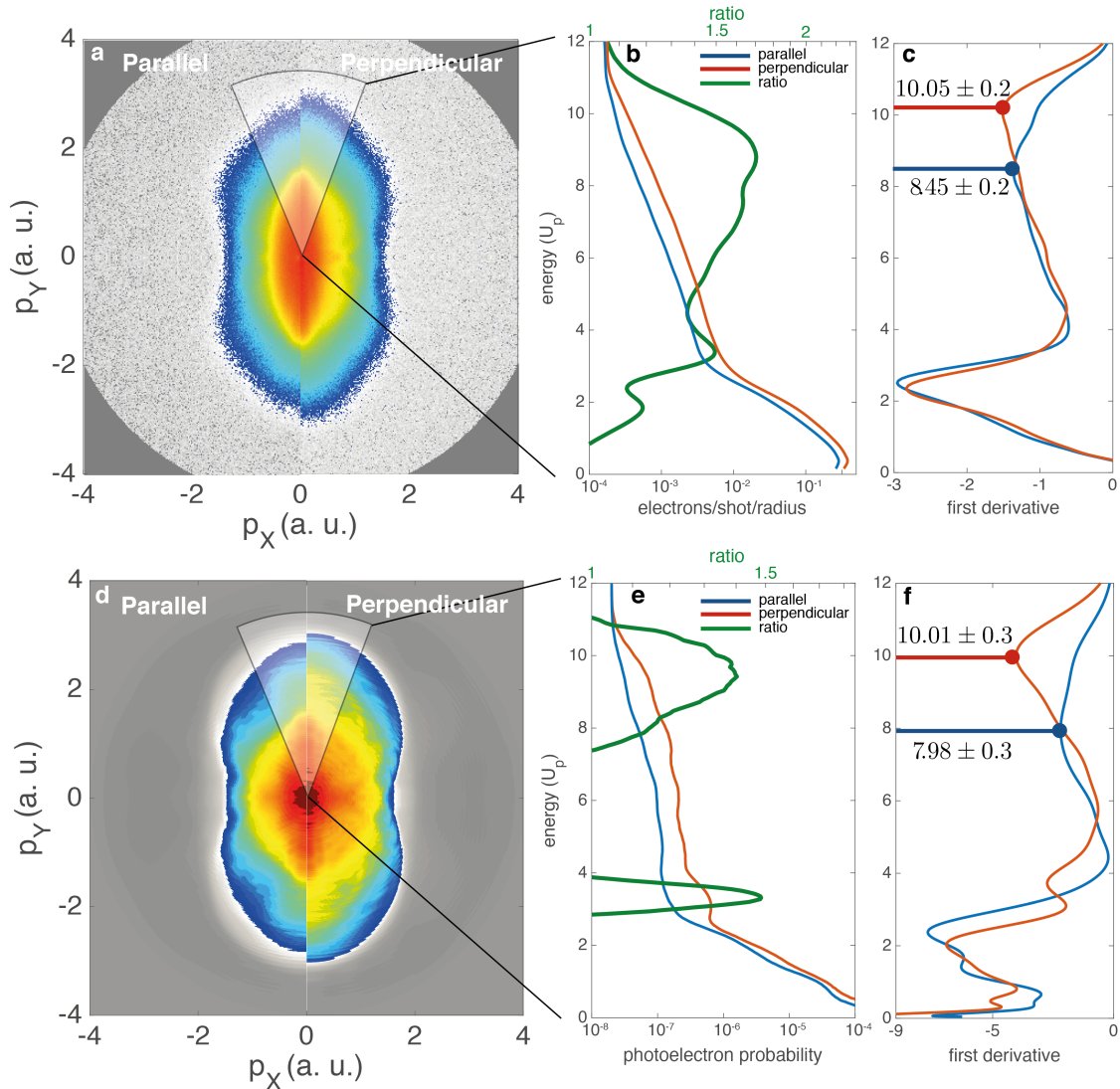


FIG. 2. Molecular-frame angle-resolved photoelectron spectra of OCS obtained **a,b,c** experimentally and **d,e,f** computationally from TDDFT calculations. **a,d**: Split graphical representation as a comparison of the photoelectron distributions for parallel and perpendicular alignment for the experimental and computational results, respectively. **b,e**: Corresponding projected energy distributions of photoelectrons along the Y axis, for a cone of $\pm 20^\circ$, as well as the ratio of the integral-normalised perpendicular and parallel distributions, on logarithmic scales. Energies are reported in units of the ponderomotive energy U_p . **c,f**: First derivatives of the photoelectron-energy distributions to evaluate the high-energy cutoff for the two molecular-alignment cases. All computational results were obtained by averaging over different laser-molecule orientations according to the experimental alignment distributions and by adding a constant to account for the experimental background level, see *Appendix*.

the energy range between $2 U_p$ and $10 U_p$, where the distribution is dominated by rescattered electrons [25]. Furthermore, the ratio increases with energy, reaching the maximum around the cutoff. To evaluate the cutoffs, the first derivative of the energy distributions are shown in Fig. 2 c and their minima were used to find the edges of the distributions, which allowed us to analyse the cutoff region. The first minima, for both alignment cases around $2 U_p$, represents the cutoff of direct electrons [25]. Surprisingly, the second minimum behaves differently for the two alignments. While it is located around $10 U_p$ for perpendicular alignment, as expected from the well

established above-threshold ionisation theory [24], the cutoff is shifted down to a value around $8.5 U_p$ for parallel alignment.

To unravel the experimental observations, state-of-the-art calculations were performed using time-dependent density-functional theory (TDDFT) [26]. The MF-ARPES probability was calculated by simulating the complete dynamics of the many-body ionisation process in real-time and real-space with the tSURFF method [27, 28]. With this technique the spectrum was obtained by computing the entire time-dependent electron dynamics, including many-body electron interactions, and collecting

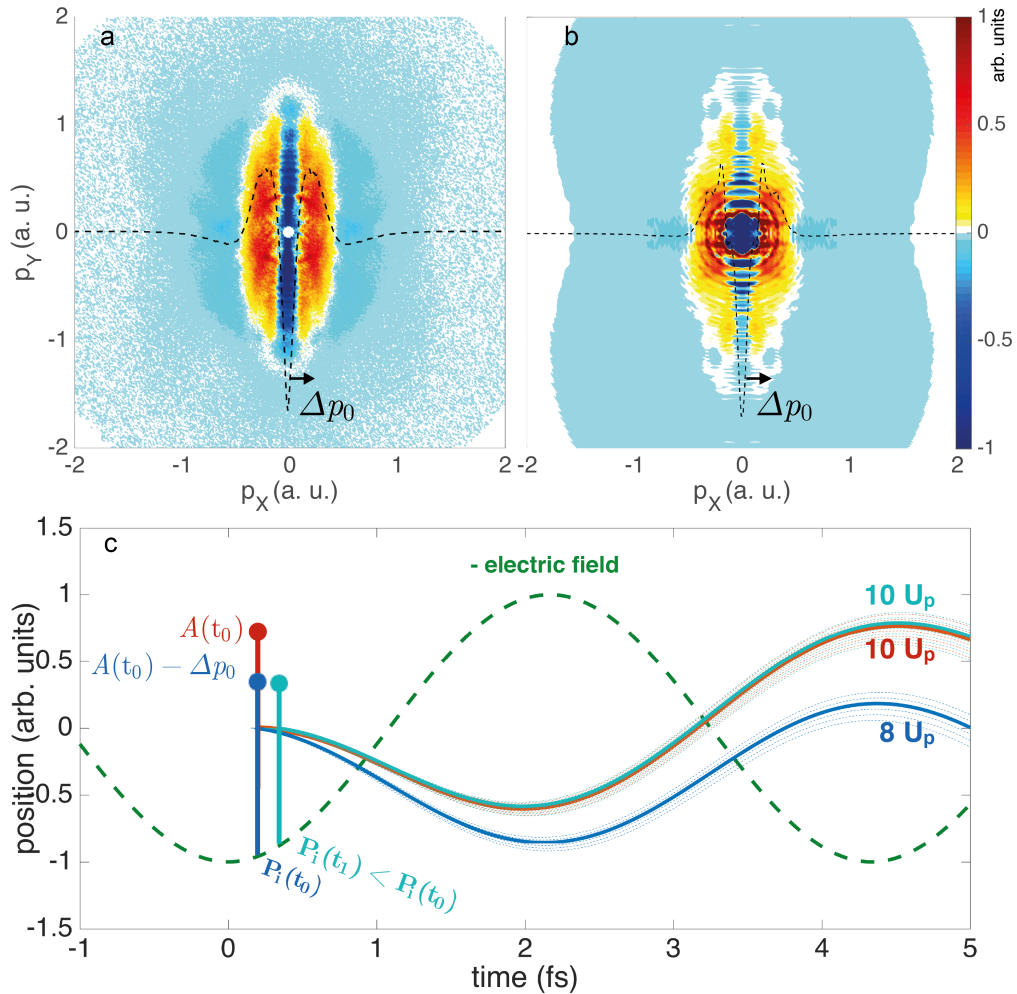


FIG. 3. **a,b**: Measured and computed differential momentum distribution (parallel – perpendicular), respectively. The signal is integrated along the Y axis to estimate the difference of transverse momentum component (black dashed line). **c**: Photoelectron trajectories calculated using our revised classical model. The green dashed line represents the external laser field, plotted as $-E_L(t)$ for clarity. A bunch of trajectories are shown for parallel (blue dashed lines) and perpendicular (red dashed lines) alignment for similar ionisation times. The optimised trajectory for perpendicular alignment leading to the $10 U_p$ cutoff is obtained for a time of ionisation t_0 (solid red curve), with the vector potential at the ionisation time $A(t_0)$. The corresponding ionisation probability is $P_i(t_0)$. For the same t_0 , the corresponding trajectory affected by the phase term Δp_0 leads to a final energy around $8 U_p$ (solid blue curve). For an ionisation time t_1 the phase shift is compensated and a trajectory following the reference trajectory from t_1 on is retrieved (solid light blue curve).

the flux of electrons through a closed surface surrounding the molecule. Fig. 2 d,e,f report the same analysis of the numerical results as performed for the experimental data in Fig. 2 a,b,c. The simulations capture the principal features of experimental data very well. In particular, Fig. 2 f shows that the calculations reproduce the experimental cutoff positions for parallel and perpendicular alignment as well as the corresponding shift between them very well. This result is strongly affected by the electron-electron interaction and the interplay between different orbitals, see *Appendix*.

Building upon the very good agreement of the independent results obtained from experiment and computation, we demonstrated that a weak perturbation of the initial

momentum acquired by the photoelectron during ionisation has a crucial effect in the overall electron dynamics and in the final kinetic energy. To have a more comprehensive picture of this initial momentum, we performed a differential analysis by subtracting the two distributions from each other. In Fig. 3 a,b the relative normalised differences, parallel minus perpendicular, are reported for the experiment and the simulation, respectively. A strong depletion along the vertical axis and two transversely off-set broad lines of positive yield appear as main features in Fig. 3 a, b, with a really good agreement between experimental and computational results. The depletion along the centerline is due to the node along the molecular axis of the degenerate Π highest occupied molecular orbital

(HOMO) of OCS; it represents a forbidden direction of electron ejection [15, 29]. Since 85 % of the HOMO electron density is localised on the CS part [29], the node perpendicular to the molecular axis is not a symmetry element and electrons can be ejected perpendicularly to the molecule. Therefore, when the molecular axis was aligned along the polarisation axis of the strong field, the electron preferentially acquired an initial transverse momentum p_{0X} that was much larger than in the case of perpendicular alignment, shown by the red vertical ridges in Fig. 3 a,b. Thus, the electron trajectory was driven away from the parent ion and the probability of rescattering was lower [15]. This explains the reduced overall signal strength of rescattered electrons for parallel alignment in Fig. 2 b,d. Here, the node and the transverse momentum were captured with unprecedented resolution. In particular, the most probable value of Δp_{0X} , the difference of p_{0X} between parallel and perpendicular alignment, could easily be retrieved by integrating the differential distribution along the Y axis, depicted by the dashed line in Fig. 3 a,b, and taking its maximum. We obtained $\Delta p_{0X} = 0.19 \pm 0.1$ a. u.; simulations are in excellent agreement with $\Delta p_{0X} = 0.185$ a. u.. For parallel alignment, we assume that $p_{0X} \gg p_{0Y}$ due to the node along the Y axis [15]. When the molecule is rotated to perpendicular alignment the total initial momentum is conserved, but the situation is inverted. Now the node is along the X axis and $p_{0X} \ll p_{0Y}$. For this reason, an observed $\Delta p_{0X} > 0$ between parallel and perpendicular alignment corresponds to a $\Delta p_{0Y} < 0$. In particular, from the previous assumption we have $|\Delta p_{0X}| \approx |\Delta p_{0Y}| \equiv \Delta p_0$, see *Appendix*, with $\Delta p_0^2/2 \approx 0.03 U_p$.

This initial momentum at the time of ionisation is usually neglected in the framework of the strong field approximation [17, 30]. We developed a revised version of the classical equation of motion used to describe strong-field processes [24], where we took into account also the initial momentum distribution. We considered the photoelectron momentum for perpendicular alignment as the reference case, see *Appendix* for the derivation of the equation. As a consequence, the trajectory of the photoelectron now depends on the molecular frame and the equation for the kinetic energy of backscattered electrons [13, eq. 7] for parallel alignment can now be written as:

$$\varepsilon_k = \frac{1}{2} \frac{E_0^2}{w^2} (\sin^2 \omega t_0 + 4 \sin \omega t_r (\sin \omega t_r - \sin \omega t_0)) + \frac{1}{2} (\Delta p_0)^2 + \frac{E_0}{w} \Delta p_0 (2 \sin \omega t_r - \sin \omega t_0) \quad (1)$$

with the amplitude of the strong laser field E_0 , the angular frequency of the laser field w , the time of ionisation t_0 , and the time of rescattering t_r , where t_r is also a function of t_0 and Δp_0 , see *Appendix*.

Fig. 3 c reports sets of photoelectron trajectories for the two molecular alignments calculated with the revised model. For perpendicular alignment, the reference case,

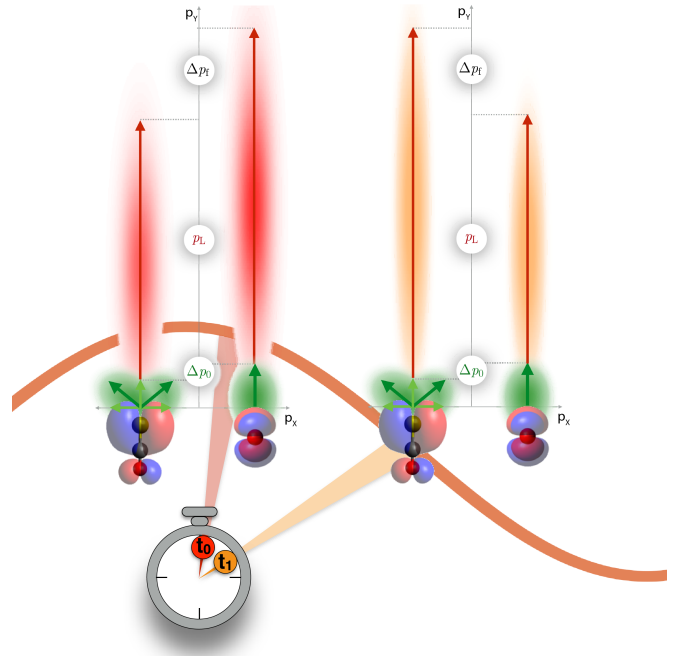


FIG. 4. Sketch of the molecular-frame-dependent dynamics of a photoelectron in the laser field when the initial momentum induced by the ionized orbital is considered.

i. e., $\Delta p_0 = 0$, the cutoff is maximised to $10 U_p$ when the molecule is photoionized around $t_0 = 180$ as after the maximum of the laser field [13], red solid line in Fig. 3 c. In this case the electron travels for ~ 3 fs before recolliding with the parent ion. When the same ionisation time t_0 is considered for parallel alignment, with $\Delta p_0 = 0.19$ a. u., we obtain a cutoff of around $8 U_p$, blue solid line in Fig. 3 c. These cutoff energies are in very good agreement with the experimental observations. It is important to note that a later ionisation time, $t_1 = 280$ as, allows the electron to reach a final kinetic energy around $10 U_p$ for the parallel alignment, light blue solid line in Fig. 3 c, but with a lower yield due to the later ionisation. In particular, the ionisation probability is now $P_i(t_1) \simeq 0.5 P_i(t_0)$, calculated by tunnelling theory [13, 29]. Furthermore, the electron born at t_1 travels for ~ 2.85 fs before recolliding with the molecule, 150 as less than the electron born at t_0 . The time spent by the photoelectron before rescattering is usually exploited as the elementary delay step for time-resolved self-diffraction experiments and it is considered to depend only on the laser wavelength [7]. Our results demonstrate that this observable is actually dependent on the molecular-frame alignment.

Within this new framework, it becomes clear that it is the molecular frame that defines the initial conditions of the electron motion in the strong laser field and this plays a major role in the photoelectron dynamics. Fig. 4 displays a sketch of the process in the XY plane, i. e., the detector view. For a given time of ionisation, different alignments of the molecular frame with respect to the

laser polarisation induce a small perturbation Δp_0 in the initial momentum of the electron. This small perturbation behaves as a phase in the dynamics of the photoelectron in the strong field and it has a major impact on its final kinetic energy. For example, if the molecule is photoionised at t_0 , the perpendicular alignment mostly supports high energy electrons, while the parallel alignment favours the emission at lower energy. For a later ionisation time t_1 the process is inverted and the parallel alignment favours high energy electrons, while the perpendicular alignment tends to produce slower electrons.

We demonstrated that the basic physics of molecular-frame strong-field ionisation is captured by considering the weak initial momentum in the dynamics of the ionised electron. This result has important impact on the seminal statements of strong-field physics. It represents an important benchmark for any self-diffraction measurement, where the fastest rescattered electrons are used to probe the structure of a molecule and the highest kinetic energy defines the spatial resolution of the structure retrieval. Our finding represents a complete breakdown of the plane wave representation usually exploited in LIED experiments [13] and points out the molecular-frame conditions as a crucial ingredient of self-diffraction experiments. This new framework is general and can be extended to a large class of molecular systems, where single ionisation from the HOMO orbital can occur and information about the initial momentum can be obtained. Furthermore, it is evident that the initial momentum sets a clock for the emission and dynamics of high-energy electrons. It highlights that the molecular frame defines the relation between the photoelectron energy and the rescattering time on a sub-fs time scale. This finding redefines the delay step of time-resolved self-diffraction experiments and opens up a new perspective on time-resolved diffraction experiments with sub-fs temporal resolution. In addition, the earliest moments of a strong-field interaction are intrinsically imprinted in the initial momentum of the electron. Thus, molecular-frame strong-field-ionisation experiments, in principle, allow one to achieve a deeper understanding of electron tunnelling, for instance, regarding the tunnelling time, on the attosecond timescale.

Besides DESY, this work has been supported by the Deutsche Forschungsgemeinschaft through the excellence cluster ‘‘The Hamburg Center for Ultrafast Imaging – Structure, Dynamics and Control of Matter at the Atomic Scale’’ (CUI, DFG-EXC1074), by the European Research Council under the European Union’s Seventh Framework Programme (FP7/2007-2013) through the Consolidator Grant COMOTION (ERC-Küpper-614507), and the Helmholtz Association Initiative and Networking Fund. A.T. and J.O. gratefully acknowledge fellowships by the Alexander von Humboldt Foundation.

Appendix

Numerical simulations

Numerical simulations of the full LIED dynamics have been performed from first-principles within the time-dependent density functional (TDDFT) [26] framework as implemented in the real-space real-time Octopus code [31]. In TDDFT, the dynamics of an interacting many-electron system is casted into the manageable problem of a fictitious non-interacting system under the effect of a time-dependent potential such that the non-interacting and the interacting systems have the same time-dependent density.

Since core electrons are expected to play marginal role in the experiment we consider only valence electrons and account for inner-shell electrons by the effect of norm-conserving Trouiller-Martins pseudopotentials. To obtain a good description of ionisation, we employed a local density approximation (LDA) functional with the average density self-interaction correction (ADSIC) [32], which corrects the asymptotic decay and provides a first ionisation energy of 11.65 eV, in good agreement with the literature [33]. During the simulations the nuclei are held fixed in the equilibrium positions, $r_{C-S} = 156.1$ pm and $r_{C-O} = 115.6$ pm.

The TDDFT equations are discretized in real-space with a cartesian grid of spacing 0.4 a. u. with a cylindrical shape of radius 50 a. u. and length 260 a. u. aligned along the laser polarisation direction. The solution of the electrons dynamics is obtained by using a discretized real-time evolution with a time step of 0.08 a. u.. The calculations are performed with a 30 fs laser pulse with the same profile as in the experiment. Complex absorbing boundaries of varying thicknesses, 40 a. u. from the caps of the cylinder and 10 a. u. on the radial borders, are placed at the edges of the simulation box to prevent spurious reflections [34].

The photoelectron spectrum is calculated by collecting the flux of the photoionisation current through a spherical surface of radius 40 a. u. with the tSURFF method [27, 28]. This approach gives access to the momentum resolved photoelectron probability $I(\mathbf{p})$ from which, by integrating along the direction perpendicular to the detector, it is possible to obtain the angular distribution of the experiment: $I(p_X, p_Y) = \int dp_Z I(\mathbf{p})$.

The indetermination of the molecular alignment in the laboratory frame is accounted for by sampling the relative angle θ between the laser polarisation and the molecular axis from 0° to 90° in steps of 10° . This procedure requires a separate simulation for each θ . The photoelectron spectra for a given configuration (parallel or perpendicular) are obtained by averaging the photoelectron distributions $I_\theta(\mathbf{p})$ with weights $n_\theta(\theta - \theta^{\parallel/\perp}) = \exp(-\sin(\theta - \theta^{\parallel/\perp})^2/(2\sigma^2))$, $\sigma^2 = 1 - \langle \cos^2\theta_{2D} \rangle$, and

$$\langle \cos^2 \theta_{2D} \rangle = 0.9.$$

Furthermore, to account for the rotation of the molecule about the polarisation axis we impose cylindrical symmetry of the photoelectron distribution about Y by averaging over ϕ : $\bar{I}_\phi(\mathbf{p}) = (2\pi)^{-1} \int_0^{2\pi} d\phi R_\phi(I(\mathbf{p}))$ with the operator R_ϕ of rotation in the X, Z plane.

The final spectrum is obtained as follows:

$$\bar{I}^{\parallel/\perp}(p_X, p_Y) = \int dp_z \int d\theta n(\theta - \theta^{\parallel/\perp}) \bar{I}_{\phi, \theta}(\mathbf{p}). \quad (2)$$

To account for experimental-background in the simulations, a constant offset of 2×10^{-8} was added to the energy distributions. We point out that the background correction shifts the numerically obtained cutoffs to lower energy, but does not effect the general behaviour nor the difference of the cutoffs between the parallel and perpendicular configurations.

From the numerical simulations the crucial role of the usually neglected electron-electron interaction for correctly describing the cutoff region in the parallel configuration became evident. The decomposed contributions of the Kohn-Sham HOMO and HOMO-1 orbitals highlight their distinct contributions to two distinct cutoffs, which are strongly separated in intensity. In particular, the faint $10 U_p$ cutoff for the parallel case actually appears to be uniquely determined by the HOMO-1, which does not have a node along the molecular axis, whereas contributions from the HOMO were strongly suppressed by the presence of a node along the molecular axis, i. e., parallel to the laser-polarisation axis. Second, the independent particle simulation obtained by propagating the system with the Hartree, exchange, and correlation potentials *frozen*, as done by the widely used single-active electron model, presents a qualitatively different picture. In particular the contribution of the HOMO-1 is highly overestimated and for the parallel alignment the $10 U_p$ cutoff is restored, in clear contradiction with the experiment. These results also confirm the importance of the coherent interaction between different orbitals in strong-field ionisation [35].

Modified three-step model

We define $p_0 = \sqrt{\langle p(t_0)^2 \rangle}$ as the most probable value of the momentum distribution at the ionisation time t_0 , see Fig. 4. We define the quantities as p_0^\perp and p_0^\parallel for perpendicular and parallel alignment, i. e., the molecular axis perpendicular and parallel to Y , respectively, and obtain

$$\begin{aligned} p_0^\perp &\approx p_{0,Y}^\perp \\ p_0^\parallel &\approx p_{0,X}^\parallel \end{aligned} \quad (3)$$

Experimentally, $p_{0,X}^\parallel > p_{0,X}^\perp$; with $\Delta p_{0X} = p_{0,X}^\parallel - p_{0,X}^\perp$ and $p_0^\perp = p_0^\parallel$, we can assume that $|\Delta p_{0Y}| \sim |\Delta p_{0X}|$, which we write Δp_0 .

In a laser field $\mathbf{E}_L(\mathbf{t}) = E_0 \cos wt \hat{\mathbf{Y}}$ with the angular frequency w , the equation of motion for an electron along the Y axis (in atomic units) is:

$$a_Y(t) = a(t) = -E_0 \cos wt \quad (4)$$

Integrating (4) for the two alignment cases yields

$$\begin{aligned} p^\perp(t) &= -\frac{E_0}{w} \sin wt + \frac{E_0}{w} \sin wt_0 + p_{0,Y}^\perp \\ p^\parallel(t) &= -\frac{E_0}{w} \sin wt + \frac{E_0}{w} \sin wt_0 + p_{0,Y}^\parallel \end{aligned} \quad (5)$$

With the vector potential of the external field A this can be rewritten as

$$\begin{aligned} p^\perp(t) &= A(t) - A^\perp(t_0) \\ p^\parallel(t) &= A(t) - A^\parallel(t_0) \\ A^\parallel(t_0) &= A^\perp(t_0) + \Delta p_0 \end{aligned} \quad (6)$$

(5) and (6) show that the initial momentum distribution contributes to the dynamics of the electron along the polarisation axis of the external field. In particular, different orientations of the ionised molecular orbital with respect to the polarisation axis result in electron trajectories launched into the continuum with a different initial phase.

To demonstrate this, we consider the electron momentum for perpendicular alignment as the reference case:

$$\begin{aligned} p^\perp(t) &= A(t) - A(t_0) \\ p^\parallel(t) &= A(t) - A(t_0) - \Delta p_0 \\ &= A(t) - (A(t_0) + \Delta p_0) \\ &= A(t) - A'(t_0) \end{aligned} \quad (7)$$

We expect the photoelectron to reach the maximum kinetic energy when the ionisation occurs shortly after a maximum of the electric field $E_L(t)$ [13]. Without loss of generality, we further consider $E_L(t) > 0$. Thus $A(t_0) < 0$ and $|A(t_0)| > |A'(t_0)|$, i. e., the vector potential at the time of ionisation is smaller when $\Delta p_0 \neq 0$. Integrating (7) yields the electron trajectory

$$\begin{aligned} x^\perp(t) &= \frac{E_0}{w^2} (\cos wt - \cos wt_0) \\ &\quad + \frac{E_0}{w} \sin wt_0 (t - t_0) \\ x^\parallel(t) &= \frac{E_0}{w^2} (\cos wt - \cos wt_0) \\ &\quad + \left(\frac{E_0}{w} \sin wt_0 - \Delta p_0 \right) (t - t_0) \end{aligned} \quad (8)$$

The right side of (8) consists of, first, an oscillatory term and, second, a drift term that depends on the value of $A(t_0)$. In this case the term Δp_0 works as a phase shift in the electron trajectory, as depicted by the blue and red trajectories in Fig. 3.

For later ionisation times $|A(t_1)| > |A(t_0)|$ there exists a $t_1(t_0, \Delta p_0)$ for which:

$$|A'(t_1)| = |A(t_1) + \Delta p_0| = |A(t_0)| \quad (9)$$

For this ionisation time t_1 the phase shift is compensated and a trajectory following the reference trajectory from t_1 on is retrieved, shown as solid light-blue line in Fig. 3 c. However, the laser field is weaker, $|E_L(t_1)| < |E_L(t_0)|$ and, therefore, the ionisation probability P_i is reduced, $P_i(t_1) \ll P_i(t_0)$, which results in the lower-energy cutoff in the photoelectron spectrum.

-
- [1] P. B. Corkum, “Plasma perspective on strong-field multiphoton ionization,” *Phys. Rev. Lett.* **71**, 1994–1997 (1993).
- [2] P. B. Corkum, M. Y. Ivanov, and J. S. Wright, “Sub-femtosecond processes in strong laser fields,” *Annu. Rev. Phys. Chem.* **48**, 387–406 (1997).
- [3] F. Calegari, D. Ayuso, A. Trabattoni, L. Belshaw, S De Camillis, S Anumula, F Frassetto, L Poletto, A Palacios, P Decleva, J B Greenwood, F Martín, and M Nisoli, “Ultrafast electron dynamics in phenylalanine initiated by attosecond pulses.” *Science* **346**, 336–339 (2014).
- [4] Franck Lépine, Misha Y Ivanov, and Marc J J Vrakking, “Attosecond molecular dynamics: fact or fiction?” *Nat. Photon.* **8**, 195–204 (2014).
- [5] P. M. Kraus, B. Mignolet, D. Baykusheva, A. Rupenyan, L. Horný, E. F. Penka, G. Grassi, O. I. Tolstikhin, J. Schneider, F. Jensen, L. B. Madsen, A. D. Bandrauk, F. Remacle, and H. J. Wörner, “Measurement and laser control of attosecond charge migration in ionized iodoacetylene,” *Science* **350**, 790–795 (2015).
- [6] P. B. Corkum and F. Krausz, “Attosecond science,” *Nat. Phys.* **3**, 381–387 (2007).
- [7] Cosmin I Blaga, Junliang Xu, Anthony D DiChiara, Emily Sistrunk, Kaikai Zhang, Pierre Agostini, Terry A Miller, Louis F DiMauro, and C D Lin, “Imaging ultrafast molecular dynamics with laser-induced electron diffraction,” *Nature* **483**, 194–197 (2012).
- [8] Michael G. Pullen, Benjamin Wolter, Anh-Thu Le, Matthias Baudisch, Michael Hemmer, Arne Senftleben, Claus Dieter Schroter, Joachim Ullrich, Robert Moshhammer, C. D. Lin, and Jens Biegert, “Imaging an aligned polyatomic molecule with laser-induced electron diffraction,” *Nat. Commun.* **6**, 7262 (2015).
- [9] B Wolter, M G Pullen, A T Le, M Baudisch, K Doblhoff-Dier, A Senftleben, M Hemmer, C D Schroter, J Ullrich, T Pfeifer, R Moshhammer, S Gräfe, O Vendrell, C D Lin, and J Biegert, “Ultrafast electron diffraction imaging of bond breaking in di-ionized acetylene,” *Science* **354**, 308–312 (2016).
- [10] S G Walt, B N Ram, M Atala, N I Shvetsov-Shilovski, A von Conta, D Baykusheva, M Lein, and H J Wörner, “Dynamics of valence-shell electrons and nuclei probed by strong-field holography and rescattering,” *Nat. Commun.* **8**, 15651 (2017).
- [11] P. Ecker, A. N. Pfeiffer, C. Cirelli, A. Staudte, R. Dörner, H. G. Muller, M. Büttiker, and U. Keller, “Attosecond ionization and tunneling delay time measurements in helium,” *Science* **322**, 1525–1529 (2008).
- [12] M Meckel, A Staudte, S Patchkovskii, D M Villeneuve, P B Corkum, R Dörner, and M Spanner, “Signatures of the continuum electron phase in molecular strong-field photoelectron holography,” *Nat. Phys.* **10**, 594–600 (2014).
- [13] Zhangjin Chen, Anh-Thu Le, Toru Morishita, and C. D. Lin, “Quantitative rescattering theory for laser-induced high-energy plateau photoelectron spectra,” *Phys. Rev. A* **79**, 033409 (2009).
- [14] J. Xu, C. I. Blaga, K. Zhang, Y. H. Lai, C. D. Lin, T. A. Miller, P. Agostini, and L. F. DiMauro, “Diffraction using laser-driven broadband electron wave packets,” *Nat. Commun.* **5**, 4635 (2014).
- [15] Manfred Lein, “Antibonding molecular orbitals under the influence of elliptically polarized intense light,” *J. Phys. B* **36**, L155 (2003).
- [16] H. Niihara, F. Legare, R. Hasbani, A. D. Bandrauk, M. Y. Ivanov, D. M. Villeneuve, and P. B. Corkum, “Sub-laser-cycle electron pulses for probing molecular dynamics,” *Nature* **417**, 917–922 (2002).
- [17] M. Busuladžić, A. Gazibegović-Busuladžić, D. B. Milošević, and W. Becker, “Angle-resolved high-order above-threshold ionization of a molecule: Sensitive tool for molecular characterization,” *Phys. Rev. Lett.* **100**, 203003 (2008).
- [18] M. G. Pullen, B. Wolter, A. T. Le, M. Baudisch, M. Sclafani, H. Pires, C. D. Schröter, J. Ullrich, R. Moshhammer, T. Pfeifer, C. D. Lin, and J. Biegert, “Influence of orbital symmetry on diffraction imaging with rescattering electron wave packets,” *Nat. Commun.* **7**, 11922 (2016).
- [19] Noslen Suárez, Alexis Chacón, Marcelo F. Ciappina, Benjamin Wolter, Jens Biegert, and Maciej Lewenstein, “Above-threshold ionization and laser-induced electron diffraction in diatomic molecules,” *Phys. Rev. A* **94**, 043423 (2016).
- [20] Ming-Ming Liu, Min Li, Chengyin Wu, Qihuang Gong, André Staudte, and Yunqian Liu, “Phase structure of strong-field tunneling wave packets from molecules,” *Phys. Rev. Lett.* **116**, 163004 (2016).
- [21] Yuan-Pin Chang, Daniel A. Horke, Sebastian Trippel, and Jochen Küpper, “Spatially-controlled complex molecules and their applications,” *Int. Rev. Phys. Chem.* **34**, 557–590 (2015), arXiv:1505.05632 [physics].
- [22] Sebastian Trippel, Terence Mullins, N L M Müller, Jens S Kienitz, Juan J Omiste, Henrik Stapelfeldt, Rosario González-Férez, and Jochen Küpper, “Strongly driven quantum pendulum of the carbonyl sulfide molecule,” *Phys. Rev. A* **89**, 051401(R) (2014), arXiv:1401.6897 [quant-ph].
- [23] Y Huisman, A Rouzee, A Gijsbertsen, J H Jungmann, A S Smolkowska, P S W M Logman, F Lepine, C Cauchy, S Zamith, T Marchenko, J M Bakker, G Berden, B Redlich, Alexander F G Van Der Meer, Harm G Muller, W Vermin, K J Schafer, M Spanner, M Yu Ivanov, O Smirnova, D Bauer, S V Popruzhenko, and M J J Vrakking, “Time-resolved holography with photoelectrons,” *Science* **331**, 61–64 (2011).
- [24] G. G. Paulus, W. Becker, W. Nicklich, and H. Walther, “Rescattering effects in above threshold ionization: a classical model,” *J. Phys. B* **27**, L703–L708 (1994).
- [25] W. Becker, F. Grasbon, R. Kopold, D. B. Milošević, G. G.

- Paulus, and H. Walther, “Above-threshold ionization: From classical features to quantum effects,” *Adv. Atom. Mol. Opt. Phys.* **48**, 35–98 (2002).
- [26] Miguel A L Marques, Neepa T Maitra, F Nogueira, Eberhard K U Gross, and Angel Rubio, *Fundamentals of Time-Dependent Density Functional Theory*, Lecture Notes in Physics (Springer Verlag, 2011).
- [27] Liang Tao and Armin Scrinzi, “Photo-electron momentum spectra from minimal volumes: the time-dependent surface flux method,” *New J. Phys.* **14**, 013021 (2012).
- [28] Philipp Wopperer, Umberto De Giovannini, and Angel Rubio, “Efficient and accurate modeling of electron photoemission in nanostructures with TDDFT,” *Eur. Phys. J. D* **90**, 1307 (2017).
- [29] Lotte Holmegaard, Jonas L. Hansen, Line Kalhøj, Sofie Louise Kragh, Henrik Stapelfeldt, Frank Filsinger, Jochen Küpper, Gerard Meijer, Darko Dimitrovski, Mahmoud Abu-samha, Christian P. J. Martiny, and Lars Bojer Madsen, “Photoelectron angular distributions from strong-field ionization of oriented molecules,” *Nat. Phys.* **6**, 428 (2010), arXiv:1003.4634 [physics].
- [30] M. Lewenstein, P. Balcou, M. Y. Ivanov, A. L’Huillier, and P. B. Corkum, “Theory of high-harmonic generation by low-frequency laser fields,” *Phys. Rev. A* **49**, 2117–2132 (1994).
- [31] Xavier Andrade, David Strubbe, Umberto De Giovannini, Ask Hjorth Larsen, Micael J T Oliveira, Joseba Alberdi-Rodriguez, Alejandro Varas, Iris Theophilou, Nicole Helbig, Matthieu J Verstraete, Lorenzo Stella, Fernando Nogueira, Alán Aspuru-Guzik, Alberto Castro, Miguel A L Marques, and Angel Rubio, “Real-space grids and the octopus code as tools for the development of new simulation approaches for electronic systems,” *Phys. Chem. Chem. Phys.* **17**, 31371 (2015).
- [32] C Legrand, Eric Suraud, and P G Reinhard, “Comparison of self-interaction-corrections for metal clusters,” *J. Phys. B-Atom. Mol. Opt.* **35**, 1115 (2002).
- [33] L S Wang, J E Reutt, Y T Lee, and D A Shirley, “High-resolution uv photoelectron-spectroscopy of CO_2^+ , COS^+ and CS_2^+ using supersonic molecular-beams,” *J. Electron. Spectrosc. Relat. Phenom.* **47**, 167–186 (1988).
- [34] Umberto De Giovannini, Ask Hjorth Larsen, and Angel Rubio, “Modeling electron dynamics coupled to continuum states in finite volumes with absorbing boundaries,” *Eur. Phys. J. D* **88**, 1–12 (2015).
- [35] H Akagi, T Otobe, A Staudte, A Shiner, F Turner, Reinhard Dörner, D Villeneuve, and P Corkum, “Laser tunnel ionization from multiple orbitals in HCl,” *Science* **325**, 1364–1367 (2009).